

Spontaneous spin-polarized current in a nonuniform Rashba interaction system

 Qing-feng Sun^{1,*} and X. C. Xie^{2,3}
¹Beijing National Lab for Condensed Matter Physics and Institute of Physics, Chinese Academy of Sciences, Beijing 100080, China

²Department of Physics, Oklahoma State University, Stillwater, Oklahoma 74078, USA

³International Center for Quantum Structures, Chinese Academy of Sciences, Beijing 100080, China

(Received 23 November 2004; revised manuscript received 30 December 2004; published 27 April 2005)

We investigate electron transport through a two-dimensional semiconductor with a nonuniform Rashba spin-orbit interaction. Due to the combination of the coherence effect and the Rashba interaction, a spontaneous spin-polarized current emerges in the absence of any magnetic material and magnetic field. For a two-terminal device, only the local current contains polarization; however, with a four-terminal setup, a polarized total current is produced. This phenomenon may offer a different way to generate a spin-polarized current, in addition to the traditional spin-injection method.

DOI: 10.1103/PhysRevB.71.155321

PACS number(s): 73.21.Hb, 72.25.Dc, 75.47.-m

How to generate a spin-polarized current in a semiconductor (SC) has been one of the most significant and challenging issues in condensed matter physics.¹⁻³ Apart from the fundamental physics interest, it may also have direct commercial applications. Over the past several years, the issue has attracted great experimental and theoretical efforts. Due to the fact that semiconductors are in general spin unpolarized, the key for generating polarized current in previous works was through spin injection, namely, to produce spin-polarized electrons from a polarized source [e.g., a ferromagnet (FM) or polarized photon] and then inject them into a SC. However, among the currently existing spin-injection methods,^{1,3} none is very satisfactory. For the spin injection from a FM to a SC, its spin-polarization efficiency is usually low with a typical polarization of around 1%.⁴ For the polarized optical methods of spin injection, it is difficult to integrate with electronic devices.⁵

Very recently, based on the Rashba spin-orbit (SO) interaction, some theoretical works proposed different approaches to generating a spin-polarized current without FM materials.⁶⁻⁸ For example, Ionicioiu and D'Amico proposed a spin-polarizing device consisting of a Mach-Zehnder interferometer with a Rashba SO interaction on one arm and a threading magnetic flux passing the ring.^{6,9} The Rashba SO interaction is an intrinsic interaction in a two-dimensional electron system (2DES) of SC heterostructures.^{10,11} It originates from an asymmetrical-interface electric field, i.e., the asymmetrical potential energy in the direction perpendicular to the interface. The strength of the Rashba interaction can be tuned and controlled by an external electric field or gate voltage.¹²

In this paper, we predict that a spin-polarized current spontaneously emerges in the SC in the presence of a nonuniform Rashba SO interaction. In particular, this spin-polarized current is an intrinsic property of the nonuniform Rashba SC, and it does not need any magnetic materials or a magnetic field. While under a voltage bias, a local polarized current is produced everywhere, but with zero total polarized current. However, for an open multiterminal setup, a total polarized current emerges. Thus, our proposal offers an efficient and simple method to generate a spin-polarized current.

We first show the principle of generating a spin-polarized

current. For simplicity, we assume two paths for an electron traveling from one terminal of a sample to the other [see Fig. 1(a)], and t_1 and t_2 are their respective transmission coefficients. Because the Rashba interaction strength α is tunable in experiments,¹² we choose different α in the two paths. An extreme case is $\alpha=0$ in one path, e.g., path 1, and a large α in path 2. This particular choice is not essential, but it brings out the physics more clearly. Due to the Rashba interaction, an extra phase is generated when an electron passes path 2.¹³ In particular, this phase is dependent on the spin of the incident electron. For a spin-up electron, the extra phase is $\varphi = -k_R L = -\alpha m^* L / \hbar^2$ (where L is the length of path 2 and m^* is the electron effective mass), assuming that the Rashba energy is weak compared with the kinetic energy. On the other hand, the phase is $-\varphi = k_R L$ for a spin-down electron. If only to consider the first-order tunneling process, the total transmission probability for the spin-up incident electron is $T_{\uparrow} = |t_1 + t_2 e^{i\varphi}|^2$, which in general is different from that for the

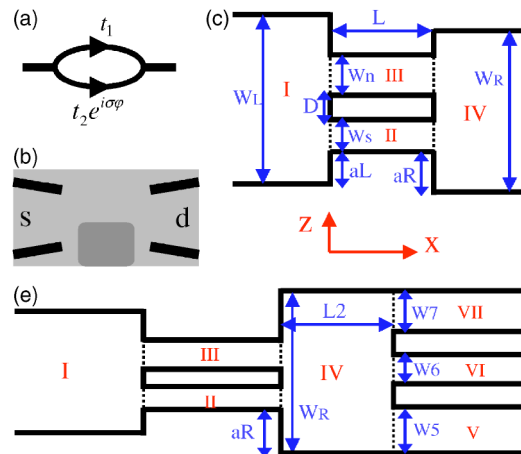


FIG. 1. (Color online) (a) Schematic diagram for an electron transport through two paths in a two-terminal device. (b) Schematic diagram for an open multiterminal device made of semiconductor 2DGS with four split gates (the black region). The Rashba interaction in the deep gray region differs from the rest of the system. (c) and (d) are the configurations for the specific two-terminal and four-terminal systems, respectively.

spin-down electron, $T_{\downarrow} = |t_1 + t_2 e^{-i\varphi}|^2$. Therefore, a spin-polarized current is spontaneously generated, and its polarization p at zero temperature is

$$p = \frac{T_{\uparrow} - T_{\downarrow}}{T_{\uparrow} + T_{\downarrow}} = \frac{2|t_1 t_2| \sin \theta \sin \varphi}{|t_1|^2 + |t_2|^2 + 2|t_1 t_2| \cos \theta \cos \varphi}, \quad (1)$$

where θ is the phase difference between t_1 and t_2 .

Next, we consider a specific two-dimensional and two-terminal SC system, shown in Fig. 1(c).¹⁴ In this device, two wires, II and III, are in the center region. In order to show that our results are general, we choose the system without the mirror symmetry. In this setup, an incident electron from terminal I traveling to terminal IV has two paths, i.e., passing region II or III. If the Rashba interaction α 's are different in regions II and III, the above-mentioned coherent effect will occur. Then a spin-polarized current should be generated, although there is no magnetic material or magnetic field.

The Hamiltonian for the two-terminal system [Fig. 1(c)] is

$$H = \frac{p_x^2 + p_z^2}{2m^*} + V(x, z) + \frac{\alpha}{\hbar} (\sigma_z p_x - \sigma_x p_z), \quad (2)$$

where $V(x, z)$ is the potential energy. Here we let $V(x, z) = 0$ in the regions I and IV, $V(x, z) = V_2$ (or V_3) in the region II (or III), and $V(x, z) = \infty$ in other regions. The last term in Eq. (2) is the Rashba interaction and $\alpha(x, z)$ describes its strength. For simplicity, we assume that $\alpha = 0$ in the regions I and IV, and $\alpha = \alpha_2$ and α_3 in the regions II and III, respectively. Boundary matching is employed to solve for the transmission coefficients.^{15,16} Assuming that the incident electron is

at the subband n with the spin index s and the energy E from terminal I, and, to neglect the mixing of the intersubband in regions II and III,^{13,17} the wave functions $\Phi(x, z)$ in the regions I to IV are written as follows:¹⁷

$$\Phi(x, y) = \begin{cases} e^{ik_r^I x} \varphi_n^I(z) s + \sum_m r_{mns} e^{-ik_r^I x} \varphi_m^I(z) s \\ \sum_m a_{mns}^+ e^{ik_{ms}^{II+} x} \varphi_m^{II}(z) s + \sum_m a_{mns}^- e^{ik_{ms}^{II-} x} \varphi_m^{II}(z) s \\ \sum_m b_{mns}^+ e^{ik_{ms}^{III+} x} \varphi_m^{III}(z) s + \sum_m b_{mns}^- e^{ik_{ms}^{III-} x} \varphi_m^{III}(z) s \\ \sum_m t_{mns} e^{ik_m^{IV} x} \varphi_m^{IV}(z) s \end{cases}.$$

$s = \uparrow / \downarrow$ or ± 1 is the spin index, and s also describes the corresponding spin states, in which $s = (1, 0)^T$ for \uparrow and $s = (0, 1)^T$ for \downarrow . $\varphi_m^\beta(z)$ ($\beta = \text{I, II, III, and IV}$) are orthonormal transverse wave functions for the subband m in the region β . $k_m^{II/IV}$ and $k_{ms}^{\gamma\pm}$ ($\gamma = \text{II or III}$) are the corresponding x -direction wave vectors with $k_m^{II/IV} = \sqrt{(2m^*/\hbar^2)(E - E_m^{II/IV})}$ and $k_{ms}^{\gamma\pm} = \pm \sqrt{(2m^*/\hbar^2)(E - V_\gamma - E_m^\gamma) + k_{R\gamma}^2 - sk_{R\gamma}}$ in which $k_{R\gamma} \equiv \alpha_\gamma m^* / \hbar^2$ and $E_m^\beta = (\hbar^2 / 2m^*) (m\pi / W)^\beta$. t_{mns} and r_{mns} are the transmission and reflection amplitudes, and a_{mns}^\pm and b_{mns}^\pm are constants to be determined by matching the boundary conditions. Here the boundary conditions are^{18,19} $\Phi(x, z)|_{x=0^-/L^-} = \Phi(x, z)|_{x=0^+/L^+}$ and $\hat{v}_x \Phi(x, z)|_{x=0^-/L^-} = \hat{v}_x \Phi(x, z)|_{x=0^+/L^+} + (2iU_0/\hbar) \Phi(0/L, z)$, where $\hat{v}_x = (p_x + \sigma_z \hbar k_R) / m^*$ is the velocity operator, and U_0 are the Schottky δ barrier potentials at the interfaces.²⁰ At the interface of $x = 0$, for example, we have from the boundary conditions,

$$\varphi_n^I(z) s + \sum_m r_{mns} \varphi_m^I(z) s = \begin{cases} 0, & 0 \leq z \leq a_L \\ \sum_m a_{mns}^+ \varphi_m^{II}(z) s + \sum_m a_{mns}^- \varphi_m^{II}(z) s, & a_L \leq z \leq a_L + W_s \\ 0, & a_L + W_s \leq z \leq zh \\ \sum_m b_{mns}^+ \varphi_m^{III}(z) s + \sum_m b_{mns}^- \varphi_m^{III}(z) s, & zh \leq z \leq zh + W_n \\ 0, & zh + W_n \leq z \leq W_L \end{cases}, \quad (3)$$

$$k_n^I \varphi_n^I(z) s - \sum_m r_{mns} k_m^I \varphi_m^I(z) s = \begin{cases} \sum_m a_{mns}^+ (k_{ms}^{II+} + sk_{R2}) \varphi_m^{II}(z) s + \sum_m a_{mns}^- (k_{ms}^{II-} + sk_{R2}) \varphi_m^{II}(z) s + \frac{2iU_0 m^*}{\hbar^2} \Phi(0, z), & a_L \leq z \leq a_L + W_s \\ \sum_m b_{mns}^+ (k_{ms}^{III+} + sk_{R3}) \varphi_m^{III}(z) s + \sum_m b_{mns}^- (k_{ms}^{III-} + sk_{R3}) \varphi_m^{III}(z) s + \frac{2iU_0 m^*}{\hbar^2} \Phi(0, z), & zh \leq z \leq zh + W_n \end{cases}, \quad (4)$$

where $zh \equiv a_L + W_s + D$. Next, multiplying $\varphi_j^*(z)s^T$ in the two sides of the Eq. (3) and then integrating over z from 0 to W_L , Eq. (3) changes into

$$-r_{jns} + \sum_m A_{jm} a_{mns}^+ + \sum_m A_{jm} a_{mns}^- + \sum_m B_{jm} b_{mns}^+ + \sum_m B_{jm} b_{mns}^- = \delta_{nj}, \quad (5)$$

where

$$A_{jm} \equiv \int_a^{a+W_s} dz \varphi_j^*(z) \varphi_m^{II}(z),$$

$$B_{jm} \equiv \int_{zh}^{zh+W_n} dz \varphi_j^*(z) \varphi_m^{III}(z).$$

Similarly, we multiply $\varphi_j^{II*}(z)s^T$ [or $\varphi_j^{III*}(z)s^T$] in the two sides of the first (or second) part of Eq. (4) and integrate over z from a_L (or zh) to $a_L + W_s$ (or $zh + W_n$). Then Eq. (4) reduces to

$$\sum_m k_m^I A_{mj} r_{mns} + \left[k_{js}^{II+} + sk_{R2} + \frac{2iU_0 m^*}{\hbar^2} \right] a_{jns}^+ + \left[k_{js}^{II-} + sk_{R2} + \frac{2iU_0 m^*}{\hbar^2} \right] a_{jns}^- = k_n^I A_{nj}, \quad (6)$$

$$\sum_m k_m^I B_{mj} r_{mns} + \left[k_{js}^{III+} + sk_{R3} + \frac{2iU_0 m^*}{\hbar^2} \right] b_{jns}^+ + \left[k_{js}^{III-} + sk_{R3} + \frac{2iU_0 m^*}{\hbar^2} \right] b_{jns}^- = k_n^I B_{nj}. \quad (7)$$

By using the same method, we also can obtain another three series of equations from the boundary conditions at $x=L$. Combining them and the series of Eqs. (5)–(7), there are six series of equations all together. From these series of equations, the six groups of unknown quantities, r_{mns} , a_{mns}^+ , a_{mns}^- , b_{mns}^+ , b_{mns}^- , and t_{mns} , can exactly be obtained straightforwardly. Notice that here all orders of reflection and tunneling processes have been included. Also notice that although the amount of the subbands in each region is infinity, we can take it as a large but finite number (e.g., 100) in the numerical calculations. We have checked that our results remain unchanged when more subbands are considered. After solving t_{mns} , the transmission probability T_s can be obtained through the relation $T_s(E) = \sum_{m,n} \theta(E - E_n^I) \theta(E - E_m^{IV}) (k_m^{IV}/k_n^I) |t_{mns}|^2$. Similarly, the current (or conductance) density at an arbitrary location (x, z) can also be obtained. For instance, the conductance density $g_{Xs}(x, z)$ in the x direction in region IV is

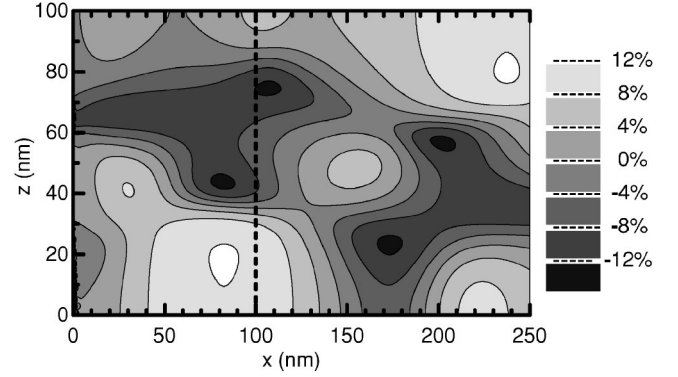


FIG. 2. The local spin polarization $p(x, z)$ vs x, z in region IV for the two-terminal device. The parameters are $V_2=0$, $V_3=-0.02$ eV, $E_F=0.013$ eV, $U=2m^*U_0/\hbar^2=0$, and $k_B T=0$.

$$g_{Xs}(x, z) = \frac{dj_{Xs}}{dV} = \frac{e^2}{h} \int dE \frac{-\partial f(E)}{\partial E} \sum_n \frac{1}{k_n} \text{Re} \left[\sum_m t_{mns}^* e^{-ik_m^{IV} x} \varphi_m^{IV}(z) \right] \times \left[\sum_m t_{mns} k_m^{IV} e^{ik_m^{IV} x} \varphi_m^{IV}(z) \right], \quad (8)$$

where $f(E) = 1 / [\exp^{(E-E_F)/k_B T} + 1]$ is the Fermi distribution function, with E_F being the Fermi energy.

We numerically study the conductance density $g_{Xs}(x, z)$ and the local spin polarization $p(x, z) \equiv [g_{X\uparrow} - g_{X\downarrow}] / [g_{X\uparrow} + g_{X\downarrow}]$. In the numerical calculations, we choose the system sizes to be $W_L = W_R = L = 100$ nm, $W_s = W_n = 30$ nm, $a_L = 0$, $a_R = 30$ nm, and $D = 10$ nm. We also set $k_{R3} = 0$ and $k_{R2} = 0.015/\text{nm}$, with the corresponding $\alpha_2 = \hbar^2 k_{R2} / m^* \approx 3 \times 10^{-11}$ eV m for $m^* = 0.036m_e$. Figure 2 shows $p(x, z)$ in region IV. Here $p(x, z)$ is clearly nonzero, and it can be over 15% at some locations. This means that the coherent effect as shown in Fig. 1(a) indeed plays a role in a finite $p(x, z)$. For a further verification, we also study the following two cases for which the coherent effect is expected to vanish: (i) closing one channel, e.g., to make region III very narrow; (ii) setting α to be equal in both regions II and III (i.e., setting $\alpha_2 = \alpha_3$). Indeed, we find $p(x, z) = 0$ in both cases for any (x, z) .

Now we show the behavior of the local spin polarization $p(x, z)$ in detail by plotting $p(x, z)$ [the red dotted curve in Fig. 3(c)] and the corresponding conductance density $g_{X\uparrow/\downarrow}$ [see Fig. 3(a)] versus z at $x = 100$ nm, i.e., the dotted-line position in Fig. 2. Figure 3(a) exhibits that $g_{X\uparrow}$ and $g_{X\downarrow}$ have a clear difference. In particular, at the peak position of $g_{X\uparrow/\downarrow}$ this difference remains, and it even reaches the largest value. Moreover, the total conductance $G_s = \int dz g_{Xs}(x, z)$ is quite large, (e.g., $G_{\uparrow} = G_{\downarrow} \approx 1.2e^2/h$ for the parameters of Fig. 2 and Figs. 3(a) and 3(b)). This means that this system can generate a large current density with a large local spin polarization. More importantly, the above property always survives, as long as the system size is within the coherent

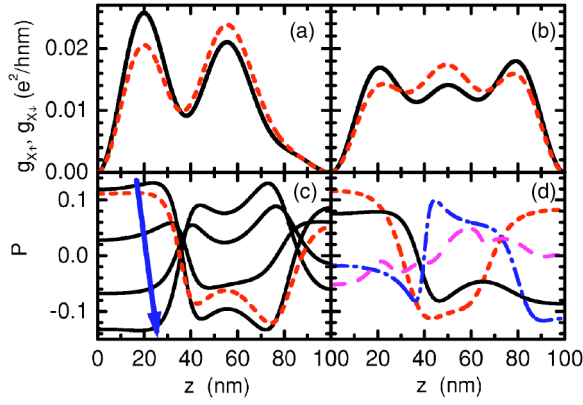


FIG. 3. (Color online) (a) and (b), $g_{x\uparrow}$ (black solid curve) and $g_{x\downarrow}$ (red dotted curve) vs z for $x=100$ nm [in (a)] and $x=1000$ nm [in (b)]. (c) $p(x, z)$ vs z for $V_3 = -0.023, -0.02, -0.026, -0.028,$ and -0.031 eV along the arrow direction. (d) $p(x, z)$ vs z for the cases of (i) $x=1000$ nm (red dotted curve), (ii) $U=0.2$ /nm (blue dash-dotted curve), (iii) $D=20$ nm and $a_R=20$ nm (black solid curve), and (iv) $E_F=0.05$ eV (magenta dashed curve). The other nomenclated parameters in (a), (b), (c), and (d) are the same as for Fig. 2 and at $x=100$ nm.

length. For example, at $x=1000$ nm, $g_{x\uparrow}$ and $g_{x\downarrow}$ still have a large difference [see Fig. 3(b)] and $p(x, z)$ can exceed $\pm 10\%$ in a wide range of z [see the red dotted curve in Fig. 3(d)].

Next we investigate how the local spin polarization $p(x, z)$ depends on sample parameters.

(i) When the potential V_3 varies slightly, $p(x, z)$ changes substantially. It can vary from the largest positive value to the largest negative value and vice versa [see Fig. 3(c)]. This characteristic is very useful. Because V_3 can be controlled by a gate voltage, $p(x, z)$ can also be tuned and controlled in an experiment.

(ii) If there exists an interface potential U_0 , $p(x, z)$ is barely affected. It may still exceed 10% [see the blue dash-dotted curve in Fig. 3(d)]. But the conductances G_s and g_{x_s} are weakened by a large U_0 .

(iii) With an increased distance D between the two channels, the overlap of the two outgoing waves from the two channels is smaller, so $p(x, z)$ will reduce slightly [see the black solid curve in Fig. 3(d)]. But $|p(x, z)|$ can still exceed 5% for $D=50$ nm.

(iv) With a larger Fermi energy E_F , more subbands in regions I–IV are available that increase G_s and g_{x_s} . Meanwhile the variation of $p(x, z)$ versus z exhibits a stronger oscillation, and its amplitude decreases slightly [see the magenta dashed curve in Fig. 3(d)].

We emphasize that although the local spin polarization $p(x, z)$ is fairly large almost everywhere,²¹ the total conductance G_s is unpolarized (i.e., $G_{\uparrow}=G_{\downarrow}$) for any two-terminal devices, because the two-terminal AB setup has a phase-locking effect.²² We prove the above statement in detail below. Due to the current conservation and the time-reversal invariance, the transmission coefficient for a two-terminal AB system without the spin degrees of freedom has the property of $T(E, \phi)=T(E, -\phi)$, the so-called phase-locking effect, where ϕ is the magnetic flux through the AB loop.²³ In our

system, since there is no spin-flip process,^{13,17} the spin-up and spin-down electrons can be treated as two independent subsystems. In the spin-up system, when an electron passes the lower channel, an extra phase $\varphi=-k_{R2}L$ is added because of the Rashba interaction.¹³ This extra phase plays the same role as if an external magnetic flux threaded the AB loop, and then we have $T_{\uparrow}(E)=T(E, \varphi)$. Similarly, for the spin-down system, a fictitious magnetic flux $-\varphi$ appears, and $T_{\downarrow}=T(E, -\varphi)$. Therefore, $T_{\uparrow}(E)=T_{\downarrow}(E)$ and $G_s=(e^2/h)\int dE[-\partial f(E)/\partial E]T_s(E)$ must be spin unpolarized, i.e., $G_{\uparrow}=G_{\downarrow}$ for any two-terminal devices.

In order to obtain a polarized total conductance (or current), we devote the rest of the paper to studying four-terminal devices. Consider a specific four-terminal device as shown in Fig. 1(d), in which the right (outgoing) terminal (the original region IV) is split into three terminals at the position $x=L+L_2$. Assuming an incident electron from terminal I, the wave function $\Phi(x, z)$ in the regions I–VII [see Fig. 1(d)] can be written similarly as it is for the two-terminal case. By matching the boundary conditions at $x=0, L,$ and $L+L_2$, the transmission amplitudes $t_{mns}^{\beta}(E)$ ($\beta=V, VI,$ and VII) from the n th subband of terminal I to the m th subband of terminal β can be exactly obtained, although the deductive process is more complicated here. Afterwards, the transmission probability $T_s^{\beta}(E)=\sum_{m,n}\theta(E-E_n^I)\theta(E-E_m^{\beta})k_m^{\beta}/k_n^I|t_{mns}^{\beta}|^2$ and the conductance $G_s^{\beta}=(e^2/h)\int dE[-\partial f(E)/\partial E]T_s^{\beta}(E)$ can also be calculated. In the numerical calculations, we choose the device geometry in the following manner: the left side and the center regions II and III are the same as for the two-terminal device, and the sizes on the right are $a_R=50$ nm, $W_5=W_7=50$ nm, $W_6=30$ nm, $W_R=200$ nm, and $L_2=100$ nm [see Fig. 1(d)]; To simplify, we set the potential energy V and the Rashba interaction α in the regions I, IV, V, VI, and VII to be zero. In a multiterminal device, the total conductance G_s^{β} and the total current are spin polarized, so we focus on G_s^{β} and its polarization p^{β} [$p^{\beta}\equiv(G_{\uparrow}^{\beta}-G_{\downarrow}^{\beta})/(G_{\uparrow}^{\beta}+G_{\downarrow}^{\beta})$], instead of the local conductance $g_{x_s}(x, z)$ and the local polarization $p(x, z)$ as in the two-terminal case.

Figures 4(a) and 4(b) show the conductance G_s^{VI} and its polarization p^{VI} versus the potential V_3 . G_{\uparrow}^{VI} and G_{\downarrow}^{VI} show a large difference. This difference can be more than $0.15e^2/h$ and p^{VI} can exceed $\pm 10\%$ in a wide range of V_3 . p^{VI} versus V_3 exhibits an oscillatory behavior. In particular, it can oscillate from a maximum positive (or negative) value to a maximum negative (or positive) value with changing V_3 . This characteristic is very useful, meaning that the spin-polarized direction and strength can be conveniently controlled in an experiment by tuning the potential V_3 . For the other two terminals V and VII, $G_s^{V/VII}$ and $p^{V/VII}$ have similar behaviors. Below we emphasize two points:

(i) It is the total conductance (or current) that is polarized, not only the conductance density with local polarization. This polarization can survive within the spin-coherent length instead of the electron-coherent length, as in the two-terminal case. Usually, the former may be much longer than the latter.²³

(ii) In the present device, the spin-polarized current is generated without a magnetic material or a magnetic field. In the zero-bias case, anywhere inside the sample is nonmag-

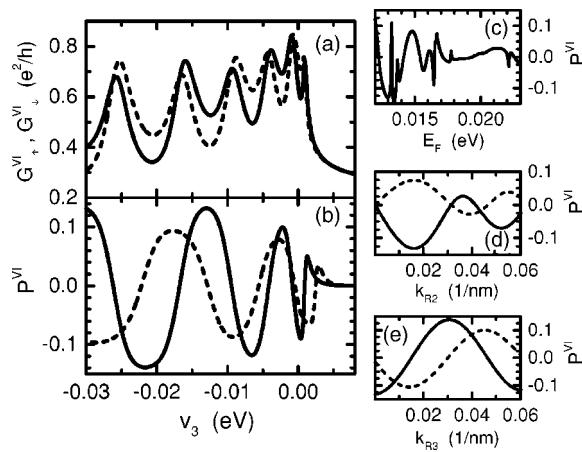


FIG. 4. (a) G_+^{VI} (solid) and G_-^{VI} (dotted) vs V_3 . (b) p^{VI} vs V_3 for $E_F=0.013$ eV (solid) and 0.015 eV (dotted). (c) p^{VI} vs E_F . (d) p^{VI} vs k_{R2} for $E_F=0.013$ eV (solid) and 0.015 eV (dotted). (e) p^{VI} vs k_{R3} for $k_{R2}=0.015/\text{nm}$ (solid) and $k_{R2}=0.03/\text{nm}$ (dotted). The other nonmentioned parameters in (a)–(e) are $V_2=0$, $V_3=-0.02$ eV, $k_{R2}=0.015/\text{nm}$, $k_{R3}=0$, and $E_F=0.013$ eV.

netic. When a bias is added, a spin-polarized current spontaneously emerges due to the coherent effect and a nonuniform Rashba interaction.

We now study how the polarization p^{VI} depends on other parameters:

(i) p^{VI} versus the Fermi energy E_F exhibits disorderlike oscillating behavior, and the amplitude slightly weakens at high E_F [see Fig. 4(c)].

(ii) p^{VI} versus k_{R2} (i.e., α_2) is a sinusoidlike curve with the period $\sim 2\pi$ [Fig. 4(d)]. But it is not an exact periodic function because the Rashba interaction also gives rise to an energy term $\hbar^2 k_R^2/2m^*$ except for the extra phase $-\sigma k_R L$.

(iii) Figure 4(e) shows p^{VI} versus k_{R3} (i.e., α_3). Clearly $k_{R3}=0$ is not essential for a nonzero p^{VI} . As long as $|k_{R3} - k_{R2}| \neq 0$, a spin-polarized current appears.

Finally, let us discuss the realizability. To add a gate [the deep gray region in Fig. 1(b)] in a SC 2DGS, one can make the Rashba interaction α in this region different from the α in other regions.¹² Then, under a bias, a local spin-polarized current is automatically induced. If four extra split gates [the black one in Fig. 1(b)] are added to form an open multiterminal device, a total spin-polarized current is generated from the source to the drain. Notice that the device in Fig. 1(b) was realized about 15 years ago.²⁴ Moreover, this device is much more open than the above-mentioned four-terminal device [Fig. 1(d)]. The phase-locking effect is more severely destroyed; hence, this kind of setup will have a much larger p . In fact, if the system is sufficiently open, then only the first-order tunneling process exists due to the current bypass effect, and the spin-polarization p can reach 100% at $|t_1| = |t_2|$ and $\theta = \varphi = \pi/2$ [see Eq. (1)].

In summary, we propose a different method for generating a spin-polarized current, in addition to the traditional spin-injection approach. Here the spin-polarized current is induced due to the combination of the quantum coherent effect and the Rashba spin-orbit interaction. In the two-terminal device, a local spin-polarized current is produced, while in an open multiterminal setup, a total spin-polarized current emerges in the absence of magnetic material or an external magnetic field.

We gratefully acknowledge financial support from the Chinese Academy of Sciences and NSFC under Grant Nos. 90303016 and 10474125. XCX is supported by US-DOE under Grant No. DE-FG02-04ER46124 and NSF-MRSEC under DMR-0080054.

*Electronic address: sunqf@aphy.iphy.ac.cn

¹S. A. Wolf, D. D. Awschalom, R. A. Buhrman, J. M. Daughton, S. V. Molnar, M. L. Roukes, A. Y. Chtchelkanova, and D. M. Treger, *Science* **294**, 1488 (2001).

²G. A. Prinz, *Science* **282**, 1660 (1998).

³I. Zutic, J. Fabian, and S. Das Sarma, *Rev. Mod. Phys.* **76**, 323 (2004).

⁴G. Schmidt, D. Ferrand, L. W. Molenkamp, A. T. Filip, and B. J. V. Wees, *Phys. Rev. B* **62**, R4790 (2000); P. C. van Son, H. van Kempen, and P. Wyder, *Phys. Rev. Lett.* **58**, 2271 (1987).

⁵I. Zutic, J. Fabian, and S. Das Sarma, *Appl. Phys. Lett.* **79**, 1558 (2001); **82**, 221 (2003).

⁶R. Ionicioiu and I. D'Amico, *Phys. Rev. B* **67**, 041307(R) (2003).

⁷V. M. Ramaglia, D. Bercioux, V. Cataudella, G. De Filippis, C. A. Perroni, and F. Ventriglia, *Eur. Phys. J. B* **36**, 365 (2003).

⁸A. A. Kiselev and K. W. Kim, *J. Appl. Phys.* **94**, 4001 (2003).

⁹Y. Ji, Y. Chung, D. Sprinzak, M. Heiblum, D. Mahalu, and H. Shtrikman, *Nature (London)* **422**, 415 (2003).

¹⁰E. I. Rashba, *Fiz. Tverd. Tela (Leningrad)* **2**, 1224 (1960) [*Solid State Ionics* **2**, 1109 (1960)].

¹¹Y. A. Bychkov and E. I. Rashba, *J. Phys. C* **17**, 6039 (1984).

¹²J. Nitta, T. Akazaki, H. Takayanagi, and T. Enoki, *Phys. Rev. Lett.* **78**, 1335 (1997); T. Matsuyama, R. Kursten, C. Meibner, and U. Merkt, *Phys. Rev. B* **61**, 15 588 (2000).

¹³S. Datta and B. Das, *Appl. Phys. Lett.* **56**, 665 (1990).

¹⁴Here we consider that the size of the device, e.g., L in Fig. 1(c) or $L+L_2$ in Fig. 1(d), is within the electron coherent length, so that the electron keeps the coherence when it passes the device, and the spin-flip process can also be determined.

¹⁵R. Shankar, *Principles of Quantum Mechanics* (Plenum Press, New York, 1980), p. 177.

¹⁶R. L. Schult, D. G. Ravenhall, and H. W. Wyld, *Phys. Rev. B* **39**, 5476 (1989); J. Wang, H. Guo, and R. Harris, *Appl. Phys. Lett.* **59**, 3075 (1991); Q. F. Sun, P. Yang, and H. Guo, *Phys. Rev. Lett.* **89**, 175901 (2002).

¹⁷When the mixture of the intersubband is neglected, σ_z is a good quantum number and the spin-flip process will not occur, so there are no terms with the spin $-s$ in the wave function $\Phi(x, z)$. If $k_R^2 W_s^2 \ll 1$, the above approximation is quite reasonable. For example, see M. H. Larsen, A. M. Lunde, and K. Flensberg, *Phys. Rev. B* **66**, 033304 (2002).

- ¹⁸Here the boundary conditions require the continuity of the velocity operator acting on the wave function instead of the derivative continuity, because $p_x\alpha(x)=\alpha(x)p_x-i\hbar(\partial/\partial x)[\alpha(x)]$, and $\alpha(x)$ is not continuous at the interface. For example, see L. W. Molenkamp, G. Schmidt, and G. E. W. Bauer, Phys. Rev. B **64**, 121202 (2001); U. Zulicke and C. Schroll, Phys. Rev. Lett. **88**, 029701 (2002).
- ¹⁹A. Szafer and A. D. Stone, Phys. Rev. Lett. **62**, 300 (1989).
- ²⁰F. Mireles and G. Kirczenow, Phys. Rev. B **66**, 214415 (2002).
- ²¹In fact, in the incident region I and the middle regions II and III, the local currents also are spin-polarized.
- ²²M. Buttiker, Phys. Rev. Lett. **57**, 1761 (1986); G. Hackenbroich, Phys. Rep. **343**, 463 (2001).
- ²³J. M. Kikkawa, and D. D. Awschalom, Phys. Rev. Lett. **80**, 4313 (1998); R. M. Potok, J. A. Folk, C. M. Marcus, and V. Umansky, *ibid.* **89**, 266602 (2002).
- ²⁴For example, see U. Meirav, M. A. Kastner, and S. J. Wind, Phys. Rev. Lett. **65**, 771 (1990).